crystals

MDPI

Article

Optical Conductivity in a Two-Dimensional Extended Hubbard Model for an Organic Dirac Electron System α-(BEDT-TTF)$_2$I$_3$

Daigo Ohki [1,*], Genki Matsuno [1], Yukiko Omori [2] and Akito Kobayashi [1]

[1] Department of Physics, Nagoya University, Furo-cho, Chikusa-ku, Nagoya 464-8602, Japan; matsuno@s.phys.nagoya-u.ac.jp (G.M.); akito@s.phys.nagoya-u.ac.jp (A.K.)
[2] Toyota College, National Institute of Technology, Eisei-cho 2-1, Toyota 471-8525, Japan; yukiko.omori@toyota-ct.ac.jp
* Correspondence: dohki@s.phys.nagoya-u.ac.jp

Received: 25 February 2018; Accepted: 14 March 2018; Published: 16 March 2018

Abstract: The optical conductivity in the charge order phase is calculated in the two-dimensional extended Hubbard model describing an organic Dirac electron system α-(BEDT-TTF)$_2$I$_3$ using the mean field theory and the Nakano-Kubo formula. Because the interband excitation is characteristic in a two-dimensional Dirac electron system, a peak structure is found above the charge order gap. It is shown that the peak structure originates from the Van Hove singularities of the conduction and valence bands, where those singularities are located at a saddle point between two Dirac cones in momentum space. The frequency of the peak structure exhibits drastic change in the vicinity of the charge order transition.

Keywords: Dirac electron; charge order; optical conductivity; organic conductor; α-(BEDT-TTF)$_2$I$_3$

1. Introduction

An organic conductor α-(BEDT-TTF)$_2$I$_3$ has attracted much interest, since it exhibits a transition between the charge order (CO) [1–7] and the massless Dirac electron (DE) [8–15] as hydrostatic pressure, P, increases. Recently, strong electron correlation effects have been revealed in both the CO [16] and the massless DE [17–20] in spin fluctuations. Thus, electron correlation effects in transport phenomena have also been expected, especially in the crossover region between the massless DE and the CO.

It has been observed that the optical gap determined by the optical conductivity decreases monotonously as P increases and reaches almost zero at about $P_c = 12$ kbar [21,22], while the resistivity gap reaches almost zero at about 7 kbar [23]. In order to explain such metallic behavior in the presence of the CO gap, metallic channels owing to edges and domain walls in the CO have been studied using the extended Hubbard model [24–27]. It has been shown that the massive DE phase with the gapless edge states emerges in the intermediate region between the massless DE phases and the trivial CO. Although the CO gap induced by the inversion symmetry breaking exists in both the massive DE phase and the trivial CO, a pair of Dirac cones with a finite gap at incommensurate momentum, $\pm\mathbf{k}_D$, merges at a time reversal invariant momentum (TRIM) at the transition between these two phases [12,15,28,29]. Such a drastic change in the band structure is expected to give rise to a characteristic in the optical conductivity.

In the present paper, the optical conductivity is calculated in the band structure determined by the mean-field theory in the extended Hubbard model for the two-dimensional electron system in the organic conductor α-(BEDT-TTF)$_2$I$_3$, where the nearest-neighbor Coulomb repulsion, V_a is used to control the charge ordering [1,2], although the donor-acceptor interactions can be also important for the charge ordering [7]. It is shown that a peak structure emerges above the CO gap in the optical

conductivity. The frequency of the peak structure, $\omega_{\rm peak}$, owing to interband excitation between two Van Hove singularities in the conduction and valence bands, rapidly moves as a nonmonotonic function of V_a, while the frequency of the CO gap, $\omega_{\rm CO}$, increases monotonically as V_a increases. Those Van Hove singularities originate from the saddle points between two Dirac cones. The optical conductivity exhibits a characteristic strong peak when two Dirac cones merge in the presence of a large CO gap.

This paper is described as follows. An extended Hubbard model for a two-dimensional electron system in α-(BEDT-TTF)$_2$I$_3$, the mean field theory, and the optical conductivity are described in Section 2. Numerical results are shown in Section 3. Sections 4 and 5 are devoted to the discussion and summary.

2. Formulation

The two-dimensional extended Hubbard model [1,2] has been used in theoretical studies for α-(BEDT-TTF)$_2$I$_3$, in order to take the on-site Coulomb repulsion, U, and the nearest-neighbor Coulomb repulsions, $V_{\alpha\beta}$, into account.

$$\begin{aligned} H &= \sum_{(i\alpha,j\beta),\sigma} (t_{(i\alpha,j\beta)}\, a^\dagger_{i\alpha\sigma} a_{j\beta\sigma} + \text{h.c.}) \\ &+ \sum_{i\alpha} U\, a^\dagger_{i\alpha\uparrow} a^\dagger_{i\alpha\downarrow} a_{i\alpha\downarrow} a_{i\alpha\uparrow} \\ &+ \sum_{(i\alpha:j\beta)} \sum_{\sigma,\sigma'} V_{i\alpha j\beta}\, a^\dagger_{i\alpha\sigma} a^\dagger_{j\beta\sigma'} a_{j\beta\sigma'} a_{i\alpha\sigma}, \end{aligned} \tag{1}$$

where $a_{i\alpha\sigma}$ and $t_{(i\alpha,j\beta)}$ represent the annihilation operators and the transfer energies with unit cells i, j, spins σ, and sublattices $\alpha, \beta =$ A, A$'$, B and C of α-(BEDT-TTF)$_2$I$_3$.

Hereafter, the energies are given in eV. The tight binding model for α-(BEDT-TTF)$_2$I$_3$ [30–34] is shown in Figure 1a. The sublattices A and A$'$ are equivalent due to the inversion symmetry in the massless DE phase. The transfer energies given by the first-principle calculation [33]: $t_{b1} = 0.1241$, $t_{b2} = 0.1296, t_{b3} = 0.0513, t_{b4} = 0.0152, t_{a1} = -0.0267, t_{a2} = -0.0511, t_{a3} = 0.0323, t'_{a1} = 0.0119$, $t'_{a3} = 0.0046$, and $t'_{a4} = 0.0060$. The nearest neighbor interaction V_a in the stacking direction is used for controlling the CO transition, because this is the most sensitive as a function of P [35–37], while we treat $U = 0.4$ and $V_b = 0.05$ as constants. The temperature $T = 0.001$ is fixed in the present paper. The lattice constants, $k_{\rm B}$ and $\hbar$ are taken as unity. The system size in numerical calculations is $N_L = 500$.

The mean-field Hamiltonian $H_{\rm MF}$ [11] is

$$H_{\rm MF} = \sum_{\mathbf{k}\alpha\beta\sigma} \tilde{\epsilon}_{\alpha\beta\sigma}(\mathbf{k}) a^\dagger_{\mathbf{k}\alpha\sigma} a_{\mathbf{k}\beta\sigma}, \tag{2}$$

$$\tilde{\epsilon}_{\alpha\beta\sigma}(\mathbf{k}) = \phi_{\alpha\sigma}\delta_{\alpha\beta} + \epsilon_{\alpha\beta}(\mathbf{k}), \tag{3}$$

$$\phi_{\alpha\sigma} = U_\alpha \langle n_{\alpha-\sigma}\rangle + \sum_{\beta'\sigma'} V_{\alpha\beta'} \langle n_{\beta'\sigma'}\rangle, \tag{4}$$

$$\epsilon_{\alpha\beta}(\mathbf{k}) = \sum_\delta t_{\alpha\beta} e^{i\mathbf{k}\cdot\delta}, \tag{5}$$

where $\phi_{\alpha\sigma}$ is the Hartree potential, $\langle n_{\alpha\sigma}\rangle = \langle a^\dagger_{i\alpha\sigma} a_{i\alpha\sigma}\rangle$ is the electron number, and δ is a vector between unit cells. The energy eigenvalues $\xi_{\gamma\sigma}(\mathbf{k})$ and the wave functions $\Phi_{\alpha\gamma\sigma}(\mathbf{k})$ are given by

$$\sum_\beta \tilde{\epsilon}_{\alpha\beta\sigma}(\mathbf{k})\, \Phi_{\beta\gamma\sigma}(\mathbf{k}) = \xi_{\gamma\sigma}(\mathbf{k})\, \Phi_{\alpha\gamma\sigma}(\mathbf{k}), \tag{6}$$

with the band index $\gamma = 1, 2, 3, 4$. The conduction and valence bands correspond to $\xi_{1\sigma}(\mathbf{k})$ and $\xi_{2\sigma}(\mathbf{k})$, respectively, since the Fermi energy is located between these two bands. The electron number $\langle n_{\alpha\sigma} \rangle$ is given by

$$\langle n_{\alpha\sigma} \rangle = \sum_{\mathbf{k}\gamma} |\Phi_{\alpha\gamma\sigma}(\mathbf{k})|^2 f(\xi_{\gamma\sigma}(\mathbf{k})), \tag{7}$$

where the Fermi distribution function is $f(\xi_{\gamma\sigma}(\mathbf{k})) = 1/(\exp[(\xi_{\gamma\sigma}(\mathbf{k}) - \mu)/k_B T] + 1)$ with the chemical potential μ determined so that the bands are 3/4-filled. Hereafter, let $E_{\gamma\sigma}(\mathbf{k}) = \xi_{\gamma\sigma}(\mathbf{k}) - \mu$ and measure the energy from μ.

The Green function $G_{\alpha\beta\sigma}(\omega, \mathbf{k})$ and the density of state $\rho(\omega)$ are given by

$$G_{\alpha\beta\sigma}(\omega, \mathbf{k}) = \sum_{\gamma} \frac{\Phi^*_{\alpha\gamma\sigma} \Phi_{\beta\gamma\sigma}}{\hbar\omega - E_{\gamma\sigma}(\mathbf{k}) + i\delta}, \tag{8}$$

$$\begin{aligned} \rho(\omega) &= \frac{1}{N_L} \sum_{\mathbf{k}\alpha\sigma} \left(-\frac{1}{\pi} \mathrm{Im} G_{\alpha\alpha\sigma}(\omega, \mathbf{k}) \right) \\ &= \frac{1}{N_L} \sum_{\mathbf{k}\alpha\gamma\sigma} \delta\left(\hbar\omega - E_{\gamma\sigma}(\mathbf{k})\right) |\Phi_{\gamma\alpha\sigma}(\mathbf{k})|^2, \end{aligned} \tag{9}$$

where N_L is the number of lattice points.

The optical conductivity is calculated by the Nakano-Kubo formula based on linear response theory. It is represented by

$$\sigma(\omega) = \frac{1}{i\omega} \left[K(\omega) - K(0) \right], \tag{10}$$

$$K(\omega) = -\frac{1}{N_L} \left(\frac{e}{\hbar} \right)^2 \sum_{\mathbf{k}\gamma\gamma'\sigma} |\mathbf{v}_{\gamma\gamma'\sigma}(\mathbf{k})|^2 \frac{f(E_{\gamma\sigma}(\mathbf{k})) - f(E_{\gamma'\sigma}(\mathbf{k}))}{E_{\gamma\sigma}(\mathbf{k}) - E_{\gamma'\sigma}(\mathbf{k}) + \hbar\omega + i\delta}, \tag{11}$$

Here, γ and σ represent a band and spin indices respectively. $\mathbf{k}$ is a wave vector. δ is a Minute amount and $\omega = E/\hbar$. where the velocity matrix $\mathrm{v}_{\gamma\gamma'\sigma}$ is calculated by

$$\mathrm{v}_{\gamma\gamma'\sigma}(\mathbf{k}) = \sum_{\alpha\beta} \Phi^*_{\alpha\gamma\sigma}(\mathbf{k}) v_{\alpha\beta\sigma}(\mathbf{k}) \Phi_{\beta\gamma'\sigma}(\mathbf{k}), \tag{12}$$

$$v_{\alpha\beta\sigma}(\mathbf{k}) = \frac{1}{\hbar} \frac{\partial}{\partial \mathbf{k}} \tilde{\epsilon}_{\alpha\beta\sigma}(\mathbf{k}). \tag{13}$$

3. Results

Figure 1b shows the conduction and valence bands in the massless DE phase. There is a pair of massless Dirac cones at incommensurate momenta, $\pm\mathbf{k}_\mathrm{D}$. The Fermi energy is located at the degenerate points of the two bands. These two bands form the tilted conical structure around $\pm\mathbf{k}_\mathrm{D}$ as shown in Figure 1c. When the energy gap between the two bands is zero, the electronic states are called as the massless DE, since quasi-particles behave as massless Dirac fermions in the relativistic quantum mechanics. There are several saddle points at the TRIMs near the Fermi energy, e.g., the M-point in the conduction band (Mc-VHS), the M-point in the valence band (Mv-VHS), and the Y-point in the valence band (Yv-VHS).

The optical conductivities at several V_a are shown in Figure 2a. These values are divided by the universal conductivity $\sigma_0 = \pi e^2/2h$ [38]. In the massless DE phase for $V_a = 0.18$, the optical conductivity almost reaches a universal constant for $k_\mathrm{B}T < \hbar\omega < \Lambda$, where $\Lambda \cong 0.01$ is a energy scale of the linear dispersion as shown in previous studies for the massless DE [38–41]. When $V > V_a^{c1} = 0.198$, a frequency of the CO gap, ω_CO, increases as V_a increases, as shown in Figure 2b, where ω_CO is defined as a flexion point of the shoulder structure in the optical conductivity. It is found that a peak structure appears above ω_CO. As presented in Figure 2b, its frequency, ω_peak, rapidly decreases as V_a increases for $V_a < V_a^{c2} = 0.212$, at which the two Dirac cones are merged in the conduction band [26,27]. In this

region, the inversion symmetry in the system is broken, and the finite gap opens near $\pm\mathbf{k}_D$ in the energy dispersion, but two Dirac cones don't merge immediately. Thus, this region of $V_a^{c1} < V_a < V_a^{c2}$ is the massive DE phase. $\omega_{\rm peak}$ rebounds after falling to $\omega_{\rm CO}$, and the optical conductivity shows a strong peak. Those two frequencies exhibit asymptotic behavior for $V_a > V_a^{c2}$, where the CO phase with the trivial gap appears.

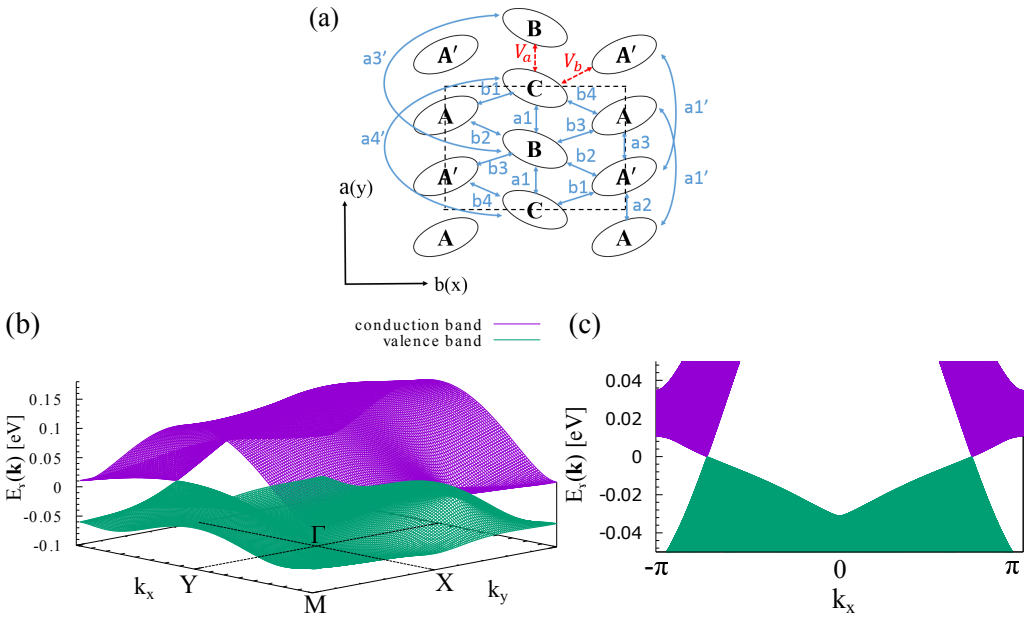

Figure 1. (**a**) Schematic figure of two-dimensional conductive plane in α-(BEDT-TTF)$_2$I$_3$. Some ellipses represent sublattices of the BEDT-TTF molecule. In the figure, signs of b1, b2, ..., a4′ correspond to transfer integrals $t_{b1}, t_{b2}, ..., t'_{a4}$ between two molecules. Nearest-neighbor Coulomb repulsions V_a, V_b are represented by the red dotted arrows. On-site Coulomb repulsion U also exists, although it is not shown in the figure. The unit cell is a region surrounded by a black dotted square in the figure. In the absence of the Coulomb interactions, the inversion symmetry points exist on B and C sublattices, and at the midpoint between A and A′ sublattices. (**b**) The conduction band (purple) and valence band (green) in the massless DE phase for $V_a = 0.18$, and (**c**) a view of same two bands projected from the side along k_x axis.

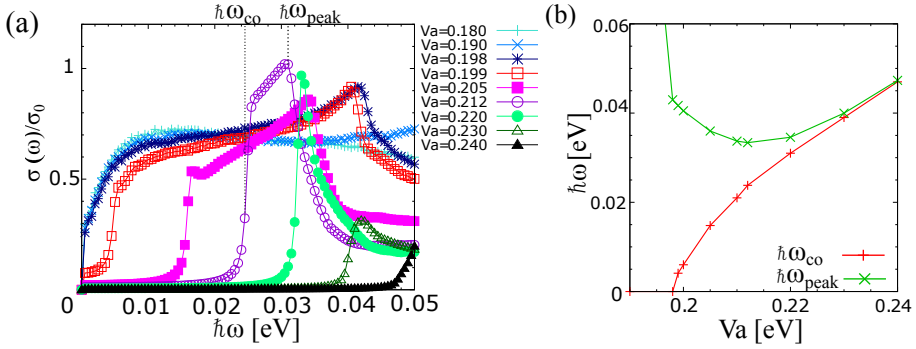

Figure 2. The optical conductivities divided by the universal conductivity $\sigma_0 = \pi e^2/2h$ [38] for $V_a = 0.180, 0.190, 0.198, 0.199, 0.205, 0.212, 0.220, 0.230, 0.240$ **(a)**. $\omega_{\rm CO}$ and $\omega_{\rm peak}$ for $V_a = V_a^{c2} = 0.212$ are shown in (**a**). V_a-dependences of $\omega_{\rm CO}$ and $\omega_{\rm peak}$ are shown in (**b**). A characteristic peak structure is found near the CO transition in the extended Hubbard model describing the organic Dirac electron system α-(BEDT-TTF)$_2$I$_3$.

Figure 3 shows the density of states $\rho(\omega)$, where the Fermi energy is defined as zero. When $V_a < V_a^{c1}$, there is a valley due to the Dirac cones. A CO gap, $\omega_{\rm CO}$, opens at the Fermi energy for $V > V_a^{c1}$.

There are several Van Hove singularities (VHS) due to saddle points of the conduction and valence bands (see Figure 1b). Here we pay attention to VHS at the M-point in the conduction band (Mc-VHS) and that in the valence band (Mv-VHS), respectively. The Mc-VHS remains an energy source for $V_a < V_a^{c2}$. Its energy rapidly increases and the peak structure disappears for $V_a > V_a^{c2}$, since it is absorbed by the upper edge of the CO gap, owing to the merging of the Dirac cones in the conduction band as shown in Figure 4. The Mv-VHS, on the other hand, moves very rapidly until it reaches the lower edge of the CO gap at V_a^{c2}. The Mv-VHS and the lower edge of the CO gap exhibits asymptotic behavior for $V_a > V_a^{c2}$. An energy difference between the Mc-VHS and Mv-VHS coincides with $\omega_{\rm peak}$ in the optical conductivity shown in Figure 2a. Other VHSs, e.g., VHS at the Y-point in the valence band (Yv-VHS), show completely different behavior as V_a increases.

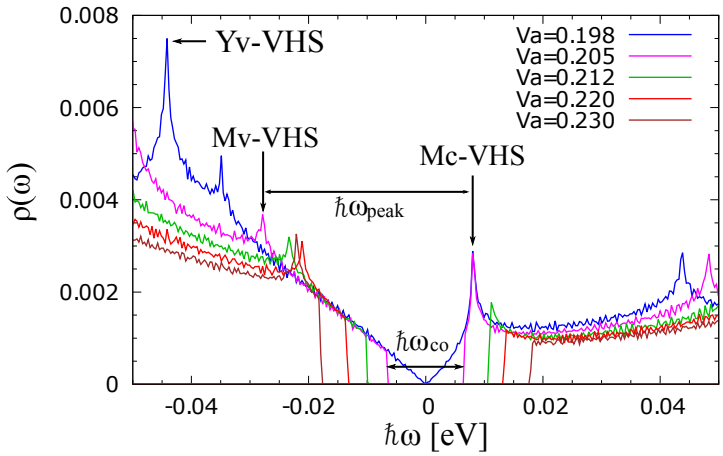

Figure 3. The density of states $\rho(\omega)$ for $V_a = 0.198, 0.205, 0.212, 0.220, 0.230$. The origin of the peak structure in the optical conductivity is identified.

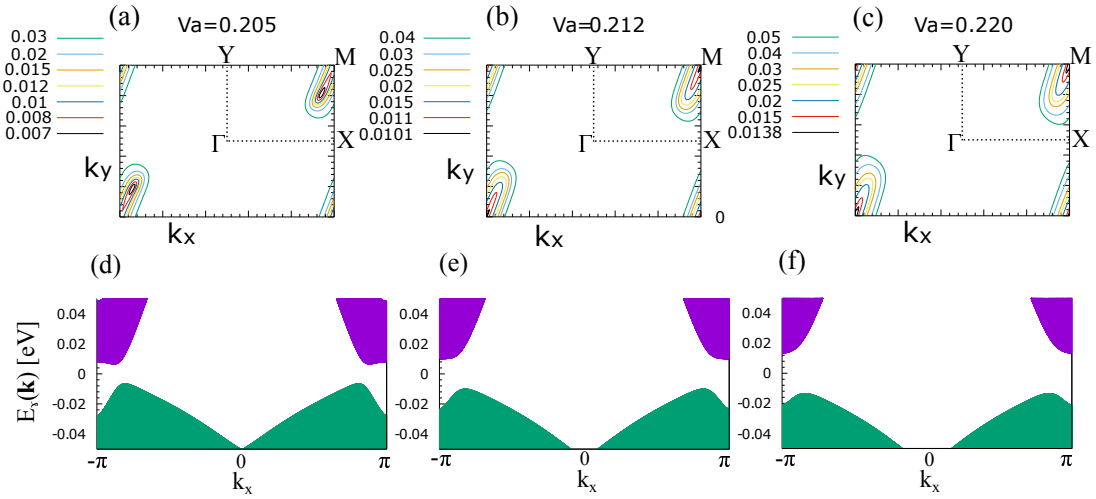

Figure 4. The contour plots of the conduction band for $V_a = 0.205$ (**a**), $V_a = V_a^{c2} = 0.212$ (**b**), and $V_a = 0.220$ (**c**). The band structures as a function of k_x for $V_a = 0.205$ (**d**), $V_a = V_a^{c2} = 0.212$ (**e**), and $V_a = 0.220$ (**f**), where the CO gaps open between the conduction bands (the purple bands) and the valence bands (the green bands). Tilting of the Dirac cones causes electron-hole asymmetric behavior as the CO gap increases.

In order to analyze the behavior of $\omega_{\rm peak}$ and $\omega_{\rm CO}$, the band structure is intensively examined in Figure 4. Both Mc-VHS and Mv-VHS exist at the M-point (the saddle point) between two Dirac cones. The Dirac cones in the conduction band (the purple band) merge at the *M*-point at V_a^{c2} in the presence of a large CO gap as shown in Figure 4b,e, leading to the absorption of the Mc-VHS into the upper

edge of the CO gap. On the other hand, the massive Dirac cones in the valence band (the green band) do not merge against relatively larger V_a as shown in Figure 4c,f, since the Dirac cones are tilted [12,13]. Thus, the Mv-VHS and the lower edge of the CO gap show asymptotic behavior.

4. Discussion

The drastic change of the optical conductivity near CO transition is characterized not only by the CO gap, but also the peak structure, as shown in Figure 2a,b. By careful analysis on the $\rho(\omega)$ shown in Figure 3 and band structure shown in Figure 4, it is elucidated that the origin of the peak structure is the VHSs at the M-points between two tilted Dirac cones. The nonmonotonic V_a-dependence of $\omega_{\rm peak}$ is due to both the merging of the Dirac cones with the CO gap and the tilting of the Dirac cones. It is expected that those features may be observed in the low frequency region (around 100 cm^{-1}), i.e., just above the CO gap near the CO transition $P_c = 12$ kbar in the optical conductivity, although this region has not been analyzed by Beyer et al. [21].

It is a future problem to investigate the optical conductivity in the non-uniform CO with the edges or the domain walls [26,27] using the real space dependent mean field theory, since it has been shown that the non-uniform CO may be important to explain the metallic CO near the CO transition [23]. The strong correlation effects beyond the mean field theory [16] may also affect the optical properties. Although the present calculation is based on the two-dimensional extended Hubbard model [1,2] being a simplest model to describe the CO in α-(BEDT-TTF)$_2$I$_3$, the donor-acceptor interactions may also play an important role for the CO [7].

5. Conclusions

The optical conductivity in the vicinity of the CO transition has been investigated using the Nakano-Kubo formula and the mean-field theory in the two-dimensional extended Hubbard model describing the Dirac electrons in α-(BEDT-TTF)$_2$I$_3$. It has been found that a peak structure above the CO gap emerges due to the two-dimensional Dirac cones. It has been also shown that the drastic change of the peak structure in the vicinity of the CO transition indicates the merging of the massive Dirac electrons. Thus it has been shown that the optical conductivity in the low frequency region just above the CO gap indicates important information on the existence of the two-dimensional massive Dirac electrons and those merging in the intermediate region between the trivial CO phase and the massless DE phase.

Acknowledgments: This work was supported by MEXT/JSPJ KAKENHI under Grant Noes 15K05166 and 15H02108.

Author Contributions: Akito Kobayashi and Yukiko Omori conceived and designed the theories; Daigo Ohki and Genki Matsuno performed the numerical calculation and analyzed the data; Daigo Ohki and Akito Kobayashi wrote the paper.

Conflicts of Interest: The authors declare no conflict of interest.

Abbreviations

The following abbreviations are used in this manuscript:

DE	Dirac electron
CO	charge order
VHS	Van Hove singularity
DOS	density of states
TRIM	time reversal invariant momentum
Mc-VHS	Van Hove singularity at the M-point in the conduction band
Mv-VHS	Van Hove singularity at the M-point in the valence band
Yv-VHS	Van Hove singularity at the Y-point in the valence band

References

1. Kino, H.; Fukuyama, H. Interrelationship among Electronic States of α-$(ET)_2I_3$, $(ET)_2MHg(SCN)_4$ and κ-$(ET)_2X$. *J. Phys. Soc. Jpn.* **1995**, *64*, 4523, doi:10.1143/JPSJ.64.4523.
2. Seo, H. Charge Ordering in Organic ET Compounds. *J. Phys. Soc. Jpn.* **2000**, *69*, 805–820.
3. Hotta, C. Classification of Quasi-Two Dimensional Organic Conductors Based on a New Minimal Model. *J. Phys. Soc. Jpn.* **2003**, *72*, 840, doi:10.1143/JPSJ.72.840.
4. Takahashi, T. ^{1}3C-NMR studies of charge ordering in organic conductors. *Synth. Met.* **2003**, *26*, 133–134, doi:10.1016/S0379-6779(02)00404-6.
5. Seo, H.; Hotta, C.; Fukuyama, T. Toward Systematic Understanding of Diversity of Electronic Properties in Low-Dimensional Molecular Solids. *Chem. Rev.* **2004**, *104*, 5005, doi:10.1021/cr030646k.
6. Kakiuchi, T.; Wakabayashi, Y.; Sawa, H.; Takahashi, T.; Nakamura, T. Charge Ordering in α-$(BEDT\text{-}TTF)_2I_3$ by Synchrotron X-ray Diffraction. *J. Phys. Soc. Jpn.* **2007**, *76*, 113702, doi:10.1143/JPSJ.76.113702.
7. Alemany, P.; Pouget, J.-P.; Canadell, E. Essential role of anions in the charge ordering transition of α-$(BEDT\text{-}TTF)_2I_3$. *Phys. Rev. B* **2012**, *85*, 195118, doi:10.1103/PhysRevB.85.195118.
8. Kajita, K.; Ojiro, T.; Fujii, H.; Nishio, Y.; Kobayashi, H.; Kobayashi, A.; Kato, R. Magnetotransport Phenomena of α-Type $(BEDT\text{-}TTF)_2I_3$ under High Pressures. *J. Phys. Soc. Jpn.* **1992**, *61*, 23, doi:10.1143/JPSJ.61.23.
9. Tajima, N.; Tamura, M.; Nishio, Y.; Kajita, K.; Iye, Y. Transport Property of an Organic Conductor α-$(BEDT\text{-}TTF)_2I_3$ under High Pressure—Discovery of a Novel Type of Conductor. *J. Phys. Soc. Jpn.* **2000**, *69*, 543–551, doi:10.1143/JPSJ.69.543.
10. Ishikawa, K.; Hirata, M.; Liu, D.; Miyagawa, K.; Tamura, M.; Kanoda, K. Spin excitations in the quasi-two-dimensional charge-ordered insulator α-$(BEDT\text{-}TTF)_2I_3$ probed via ^{1}3C NMR. *Phys. Rev. B* **2016**, *94*, 085154, doi:10.1103/PhysRevB.94.085154.
11. Kobayashi, A.; Katayama, S.; Noguchi, K.; Suzumura, Y. Superconductivity in Charge Ordered Organic Conductor –α-$(ET)_2I_3$ Salt–. *J. Phys. Soc. Jpn.* **2004**, *73*, 3135, doi:10.1143/JPSJ.73.3135.
12. Katayama, S.; Kobayashi, A.; Suzumura, Y. Pressure-Induced Zero-Gap Semiconducting State in Organic Conductor α-$(BEDT\text{-}TTF)_2I_3$ Salt. *J. Phys. Soc. Jpn.* **2006**, *75*, 054705, doi:10.1143/JPSJ.75.054705.
13. Kobayashi, A.; Katayama, S.; Suzumura, Y.; Fukuyama, H. Massless Fermions in Organic Conductor. *J. Phys. Soc. Jpn.* **2007**, *76*, 034711, doi:10.1143/JPSJ.76.034711.
14. Kajita, K.; Nishio, Y.; Tajima, N.; Suzumura, Y.; Kobayashi, A. Molecular Dirac Fermion Systems—Theoretical and Experimental Approaches—. *J. Phys. Soc. Jpn.* **2014**, *83*, 072002, doi:10.7566/JPSJ.83.072002.
15. Goerbig, M.O.; Fuchs, J.-N.; Montambaux, G.; Piéchon, F. Tilted anisotropic Dirac cones in quinoid-type graphene and α-$(BEDT\text{-}TTF)_2I_3$. *Phys. Rev. B* **2008**, *78*, 045415, doi:10.1103/PhysRevB.78.045415.
16. Tanaka, Y.; Ogata, M. Correlation Effects on Charge Order and Zero-Gap State in the Organic Conductor α-$(BEDT\text{-}TTF)_2I_3$. *J. Phys. Soc. Jpn.* **2016**, *85*, 104706, doi:10.7566/JPSJ.85.104706.
17. Hirata, M.; Ishikawa, K.; Miyagawa, K.; Tamura, M.; Berthier, C.; Basko, D.; Kobayashi, A.; Matsuno, G.; Kanoda, K. Observation of an anisotropic Dirac cone reshaping and ferrimagnetic spin polarization in an organic conductor. *Nat. Commun.* **2016**, *7*, 12666, doi:10.1038/ncomms12666.
18. Matsuno, G.; Kobayashi, A. Effect of Interband Fluctuation on Spin Susceptibility in Molecular Dirac Fermion System α-$(BEDT\text{-}TTF)_2I_3$. *J. Phys. Soc. Jpn.* **2017**, *86*, 014705, doi:10.7566/JPSJ.86.014705.
19. Hirata, M.; Ishikawa, K.; Matsuno, G.; Kobayashi, A.; Miyagawa, K.; Tamura, M.; Berthier, C.; Kanoda, K. Anomalous spin correlations and excitonic instability of interacting 2D Weyl fermions. *Science* **2017**, *358*, 1403–1406, doi:10.1126/science.aan5351.
20. Matsuno, G.; Kobayashi, A. Coexistence of velocity renormalization and ferrimagnetic fuctuation in an organic Dirac electron system α-$(BEDT\text{-}TTF)_2I_3$. accepted to *J. Phys. Soc. Jpn.* **2018**, *87*.
21. Beyer, R.; Dengl, A.; Peterseim, T.; Wackerow, S.; Ivek, T.; Pronin, A.V.; Schweitzer, D.; Dressel, M. Pressure-dependent optical investigations of α-$(BEDT\text{-}TTF)_2I_3$: Tuning charge order and narrow gap towards a Dirac semimetal. *Phys. Rev. B* **2016**, *93*, 195116, doi:10.1103/PhysRevB.93.195116.
22. Ivek, T.; Korin-Hamzić, B.; Milat, O.; Tomić, S.; Clauss, C.; Drichko, N.; Schweitzer, D.; Dressel, M. Electrodynamic response of the charge ordering phase: Dielectric and optical studies of α-$(BEDT\text{-}TTF)_2I_3$. *Phys. Rev. B* **2011**, *83*, 165128, doi:10.1103/PhysRevB.83.165128.

23. Liu, D.; Ishikawa, K.; Takehara, R.; Miyagawa, K.; Tamura, M.; Kanoda, K. Insulating nature of strongly correlated massless Dirac fermions in an organic crystal. *Phys. Rev. Lett.* **2016**, *116*, 226401, doi:10.1103/PhysRevLett.116.226401.
24. Hasegawa, Y.; Kishigi, K. Edge States in the Three-Quarter Filled System, α-(BEDT-TTF)$_2$I$_3$. *J. Phys. Soc. Jpn.* **2011**, *80*, 054707, doi:10.1143/JPSJ.80.054707.
25. Omori, Y.; Matsuno, G.; Kobayashi, A. Edge States in Molecular Solid α-(BEDT-TTF)$_2$I$_3$: Effects of Electron Correlations. *JPS Conf. Proc.* **2014**, *1*, 012119, doi:10.7566/JPSCP.1.012119.
26. Matsuno, G.; Omori, Y.; Eguchi, T.; Kobayashi, A. Topological Domain Wall and Valley Hall Effect in Charge Ordered Phase of Molecular Dirac Fermion System α-(BEDT-TTF)$_2$I$_3$. *J. Phys. Soc. Jpn.* **2016**, *85*, 094710, doi:10.7566/JPSJ.85.094710.
27. Omori, Y.; Matsuno, G.; Kobayashi, A. Longitudinal Conductivity on Edge and Domain Wall Molecular Dirac Electron System α-(BEDT-TTF)$_2$I$_3$. *J. Phys. Soc. Jpn.* **2017**, *86*, 074708, doi:10.7566/JPSJ.86.074708.
28. Montambaux, G.; Piéchon, F.; Fuchs, J.-N.; Goerbig, M.O. Merging of Dirac points in a two-dimensional crystal. *Phys. Rev. B* **2009**, *80*, 153412, doi:10.1103/PhysRevB.80.153412.
29. Montambaux, G.; Piéchon, F.; Fuchs, J.-N.; Goerbig, M.O. A universal Hamiltonian for the motion and the merging of Dirac cones in a two-dimensional crystal. *Eur. Phys. J. B* **2009**, *72*, 509, doi:10.1140/epjb/e2009-00383-0.
30. Mori, T.; Kobayashi, A.; Sasaki, Y.; Kobayashi, H.; Saito, G.; Inokuchi, H. BAND STRUCTURES OF TWO TYPES OF (BEDT-TTF)2I3. *Chem. Lett.* **1984**, *13*, 957–960, doi:10.1246/cl.1984.957.
31. Mori, T.; Mori, H.; Tanaka, S. Structural Genealogy of BEDT-TTF-Based Organic Conductors II. Inclined Molecules: θ, α, and κ Phases. *Bull. Chem. Soc. Jpn.* **1999**, *72*, 179, doi:10.1246/bcsj.72.179.
32. Kondo, R.; Kagoshima, S.; Harada, J. Crystal structure analysis under uniaxial strain at low temperature using a unique design of four-axis x-ray diffractometer with a fixed sample. *Rev. Sci. Instrum.* **2005**, *76*, 093902, doi:10.1063/1.2001607.
33. Kino, H.; Miyazaki, T. First-Principles Study of Electronic Structure in α-(BEDT-TTF)$_2$I$_3$ at Ambient Pressure and with Uniaxial Strain. *J. Phys. Soc. Jpn.* **2006**, *75*, 034704, doi:10.1143/JPSJ.75.034704.
34. Ishibashi, S.; Tamura, T.; Kohyama, M.; Terakura, K. Ab Initio Electronic-Structure Calculations for α-(BEDT-TTF)$_2$I$_3$. *J. Phys. Soc. Jpn.* **2006**, *75*, 015005, doi:10.1143/JPSJ.75.015005.
35. Kobayashi, A.; Katayama, S.; Suzumura, Y. Superconductivity in Charge Ordered Metal for Quasi-Two-Dimensional Organic Conductor. *J. Phys. Soc. Jpn.* **2005**, *74*, 2897, doi:10.1143/JPSJ.74.2897.
36. Kobayashi, A.; Katayama, S.; Suzumura, Y. Theoretical study of the zero-gap organic conductor α-(BEDT-TTF)$_2$I$_3$. *Sci. Technol. Adv. Mater.* **2009**, *10*, 024309, doi:10.1088/1468-6996/10/2/024309.
37. Tajima, N.; Kajita, K. Experimental study of organic zero-gap conductor α-(BEDT-TTF)$_2$I$_3$. *Sci. Technol. Adv. Mater.* **2009**, *10*, 024308, doi:10.1088/1468-6996/10/2/024308.
38. Stauber, T.; Peres, N.M.R.; Geim, A.K. Optical conductivity of graphene in the visible region of the spectrum. *Phys. Rev. B* **2008**, *78*, 085432, doi:10.1103/PhysRevB.78.085432.
39. Gusynin, V.P.; Sharapov, S.G.; Carbotte, J.P. Unusual Microwave Response of Dirac Quasiparticles in Graphene. *Phys. Rev. Lett.* **2006**, *96*, 256802, doi:10.1103/PhysRevLett.96.256802.
40. Suzumura, Y.; Proskurin, I.; Ogata, M. Dynamical Conductivity of Dirac Electrons in Organic Conductors. *J. Phys. Soc. Jpn.* **2014**, *83*, 094705, doi:10.7566/JPSJ.83.094705.
41. Suzumura, Y.; Proskurin, I.; Ogata, M. Reflectance of Dirac electrons in organic conductor. *J. Phys. Conf. Ser.* **2015**, *603*, 012011, doi:10.1088/1742-6596/603/1/012011.